Original Article

Prospective comparison of positron emission tomography (PET)/magnetic resonance and PET/computed tomography dosimetry in hepatic malignant neoplastic disease after ^{90}Y radioembolization treatment

Ram Gurajala[1], Sasan Partovi[1], Frank P. DiFilippo[2], Xin Li[3], Christopher Coppa[4], Shetal N. Shah[2,4], Karunakaravel Karuppasamy[1], Nancy Obuchowski[5], Ehsan Fayazzadeh[6], Gordon McLennan[7], Abraham Levitin[1]

[1]Section of Interventional Radiology, Imaging Institute, Cleveland Clinic Main Campus, Cleveland, Ohio, USA; [2]Department of Nuclear Medicine, Imaging Institute, Cleveland Clinic Main Campus, Cleveland, Ohio, USA; [3]Department of Radiology, Hospital of The University of Pennsylvania, Philadelphia, Pennsylvania, USA; [4]Section of Abdominal Imaging, Imaging Institute, Cleveland Clinic Main Campus, Cleveland, Ohio, USA; [5]Department of Quantitative Health Sciences, Cleveland Clinic Main Campus, Cleveland, Ohio, USA; [6]Department of Radiology, Saint Louis University Hospital, St. Louis, Missouri, USA; [7]Section of Interventional Radiology, Department of Radiology, University of Colorado Anschutz Medical Campus, Denver, Colorado, USA

Contributions: (I) Conception and design: All authors; (II) Administrative support: All authors; (III) Provision of study materials or patients: All authors; (IV) Collection and assembly of data: All authors; (V) Data analysis and interpretation: All authors; (VI) Manuscript writing: All authors; (VII) Final approval of manuscript: All authors.

Correspondence to: Sasan Partovi, MD. Section of Interventional Radiology, Imaging Institute, Cleveland Clinic Main Campus, 9500 Euclid Avenue, Cleveland, Ohio 44195, USA. Email: partovs@ccf.org.

Background: ^{90}Y radioembolization is an established treatment modality for hepatic malignancies. Successful radioembolization requires optimal dose delivery to tumors while minimizing dosages to parenchyma. Post-treatment positron emission tomography (PET)/computed tomography (CT) dosimetry is the established benchmark, whereas PET/magnetic resonance (MR) is an emerging modality. The goal of this study was to assess the intermodality agreement between PET/MR and PET/CT ^{90}Y dosimetry.

Methods: In this single-institution study, 18 patients (20 treatment sessions) with a primary or metastatic hepatic malignancy underwent both PET/MR and PET/CT after ^{90}Y radioembolization. Patients were randomized to undergo one modality first, followed by the other. The region of interest was delineated using MR images and tumor and liver dosimetry was calculated. Intermodality agreement was assessed using the Bland-Altman method. A generalized linear model was used to assess the effect of baseline variables on intermodality dose differences.

Results: PET/MR underestimated tumor and liver absorbed doses when compared to PET/CT by –3.7% (P=0.042) and –5.8% (P=0.029), respectively. A coverage probability plot demonstrated that 80% and 90% of tumor dose measurements fell within intermodality differences of 11% and 18%, respectively. PET/MR underestimated tumor dose at both low (<1 GBq) and high (>3 GBq) injected activity levels (P<0.001) by –22.3 [standard deviation (SD) =13.5] and –24.3 (SD =18.7), respectively.

Conclusions: Although PET/MR significantly underestimated the absorbed dose when compared to PET/CT, the intermodality agreement was high and the degree of underestimation was better than previously reported. Intermodality differences were more pronounced at low and high injected doses. Additional studies are required to assess the clinical implications of these findings.

Keywords: Positron emission tomography (PET)/magnetic resonance (MR); PET/computed tomography (PET/CT); radioembolization; hepatic malignancy; ^{90}Y dosimetry

Submitted Oct 04, 2023. Accepted for publication Jan 12, 2024. Published online Feb 26, 2024.
doi: 10.21037/jgo-23-890
View this article at: https://dx.doi.org/10.21037/jgo-23-890

Introduction

^{90}Y transarterial radioembolization (TARE) is an established therapeutic modality in the management of primary and metastatic hepatic malignancies (1,2). ^{90}Y dosimetry is a key component of ^{90}Y TARE treatment (*Figure 1*). Qualitatively, it can help assess treatment dose to liver tumor(s) and detect nontarget hepatic delivery. Quantitatively, it can determine tumor and nontumor doses to the liver to help establish dose-response and dose-toxicity relationships. Previous studies have shown a strong correlation between liver tumor radiation dose and improved clinical response (3,4). However, excessive radiation to a liver tumor/segment or to a lobe can lead to radioembolization-induced liver disease, gastrointestinal bleeding from ulceration, and radiation pneumonitis in the case of substantial nontarget dose delivery (5).

A variety of post-treatment dosimetry methods, including Bremsstrahlung single-photon emission computed tomography (bSPECT)/computed tomography (CT), positron emission tomography (PET)/CT, and PET/magnetic resonance (MR), have been used for post-Y90 assessment (6,7). Although bSPECT/CT has been shown to predict post-treatment response (8), this modality is technically limited given its photon scatter, collimator leakage, and continuous energy spectrum without a defined peak (thus limiting quantitative accuracy) (9). Further, bSPECT/CT provides only low-resolution images, which may fail to identify small lesions (10). An alternative to post-^{90}Y bSPECT/CT is ^{90}Y PET. ^{90}Y decays predominantly via β decay to ^{90}Zr at a 1.76-MeV excited state, with further decay occurring via electron conversion. It is estimated that 3×10^{-5} positrons are emitted per decay event, making PET a useful modality in this setting (11). Although ^{90}Y PET imaging may be degraded secondary to low true-coincidence count rate and high false-coincidences from Bremsstrahlung photons, the development of time-of-flight (TOF) technology has improved ^{90}Y PET image quality (12). In comparison to bSPECT/CT, ^{90}Y PET/CT has been shown to offer superior spatial resolution and dose quantification, particularly in smaller lesions (7,13). Therefore, ^{90}Y PET/CT is currently regarded as the benchmark post-^{90}Y dosimetry modality (14,15).

PET/MR is an emerging modality for post-^{90}Y dosimetry imaging, with an early study showing its feasibility in assessing post-treatment response (16). Benefits of PET/MR include superior soft tissue delineation for lesions and segments, as well as considerable reduction in radiation exposure (17). One major challenge of PET/MR involves difficulties in attenuation correction related to patients, scanning table, and radiofrequency coils (18,19). In addition, a substantial portion of installed PET/MR scanners, including ones used for this study, lack TOF-capable PET detectors. In this study, we therefore sought to assess the intermodality agreement between PET/MR and PET/CT for measurements of post-^{90}Y TARE dosimetry. We present this article in accordance with the TREND reporting checklist (available at https://jgo.amegroups.com/article/view/10.21037/jgo-23-890/rc).

Highlight box

Key findings

- Post-transarterial radioembolization (TARE) positron emission tomography (PET)/magnetic resonance (MR) significantly underestimated dose in comparison to PET/computed tomography (CT) although its clinical significance is yet unclear.

What is known and what is new?

- Post-TARE dosimetry can help establish better treatment design and assessment.
- PET/MR is technically feasible in post-TARE patients and underestimates dose in comparison to PET/CT.

What is the implication, and what should change now?

- Future studies are needed to improve PET/MR accuracy and assess the clinical implication of PET/MR dose underestimation.

Methods

Patients

This prospective study was conducted in accordance with the Declaration of Helsinki (as revised in 2013). The study was approved by the Institutional Review Board of the Cleveland Clinic Foundation (IRB No. 20-232), and informed consent was obtained from all individual participants. Patients with a primary or metastatic

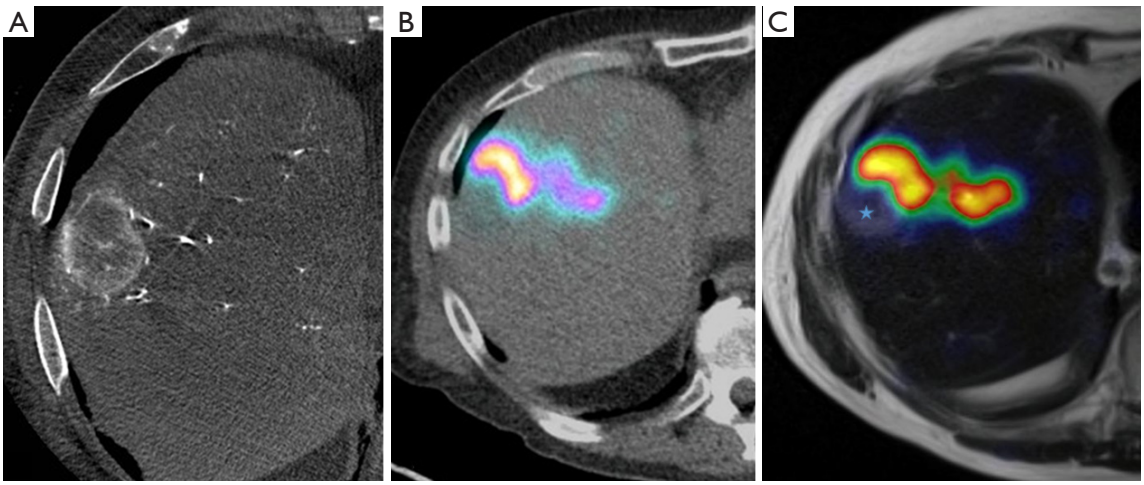

Figure 1 An example of treated tumor with radioembolization and subsequent PET/CT and PET/MR images. (A) Intraprocedural cone-beam CT image demonstrating a hypervascular segment VIII lesion. (B) Post-^{90}Y radioembolization PET/CT image cannot definitively confirm adequate tumor coverage. (C) Post-^{90}Y radioembolization PET/MR clearly demonstrates nontarget uptake medially and inadequate coverage of the lesion posterolaterally (star). PET, positron emission tomography; CT, computed tomography; MR, magnetic resonance.

hepatic malignancy who were scheduled to undergo ^{90}Y TARE between September 2019 and September 2020 were considered for inclusion in the study. Patients were excluded if they had contraindications to MR imaging, if there was a time lapse of >1 hour between PET/CT and PET/MR, and if there was a time lapse of >6 hours between the conclusion of the ^{90}Y TARE procedure and the completion of both imaging modalities. The time cut-off of 1 hour was chosen to ensure that there were no significant changes in the distribution of the embolized microspheres so direct comparisons between the modalities were feasible. The time cut-off of 6 hours was chosen to ensure optimal signal given the small branching ratio for pair positron-electron production. In addition, logistically scanning more than 6 hours after the conclusion of embolization procedure likely resulted in patients staying overnight to be scanned the day after, which was not optimal. Eighteen patients met the inclusion criteria and were included in the final study population. Of these patients, 16 underwent a single treatment session, and the remaining 2 underwent 2 treatment sessions each (for a total of 20 treatment cases).

Macroaggregated albumin (MAA) mapping and ^{90}Y radioembolization

Pre-^{90}Y mapping studies and ^{90}Y radioembolization procedures were performed according to previously described techniques (20) by seven fellowship-trained interventional radiologists with 7–10 years of clinical experience. Briefly, ^{99m}Tc-MAA was used to calculate the lung-shunt fraction and to detect excessive extrahepatic/intrahepatic shunting. Either resin or glass microspheres were then used for radioembolization depending on availability and user preference. The prescribed dose was calculated based on manufacturers' instructions for use, including Medical Internal Radiation Dosimetry for TheraSphere and body surface area or partition methods for SIR-Spheres. No advanced or personalized dosimetry was used for the study since it was not routinely performed at our institution during the study period.

Imaging protocol

After embolization, patients were randomized to undergo either PET/CT (Siemens Biograph mCT, software version VG60, Siemens Healthcare, Erlangen, Germany) or PET/MR (Siemens Biograph mMR, software version VE11, Siemens Healthcare) first, followed by the other modality within a 1-hour window. PET emission data were acquired for 20 minutes (if a single bed position covered the entire liver) or for 30 minutes (if two bed positions were needed to cover the entire liver).

Several differences between PET/CT and PET/MR were taken into consideration:

- Attenuation correction and scatter correction: PET/CT used CT images for PET data corrections,

whereas PET/MR used MR images (T1-weighted Dixon sequences) for those corrections.

- Detector timing resolution: our PET/CT system uses photomultiplier tubes and is capable of TOF imaging with a timing resolution of <0.6 ns. Our PET/MR system uses avalanche photodiodes and has a timing resolution of 4.2 ns. The PET/MR system used for this study does not support TOF imaging, although TOF compatible PET/MR system is available in the market.
- Bore size: our PET/CT system has a 78-cm bore diameter, allowing patients to be scanned with their arms up/above the head [arms-up imaging reduces attenuation and scatter in the region of interest (ROI) and improves PET image quality]. Our PET/MR system has a 60-cm bore diameter, preventing the use of arms-up imaging in several patients based on habitus. Of note, no commercially available PET/MR system has larger than 60 cm bores.
- Sensitivity and dead time: PET/MR detectors are situated closer to the patient, leading to higher sensitivity but also increased dead-time loss. PET/CT detectors are located further away from the patient, leading to lower sensitivity but decreased dead-time loss.

The PET/MR software (VE11) generated the mu-map (used for PET attenuation and scatter correction) directly from the MR T1-weighted Dixon images using a four-class segmentation model (lean tissue, fatty tissue, air, and lung). Images acquired in patients scanned with their arms down were prone to truncation artifacts.

Imaging analysis

All studies were analyzed by a fellowship-trained nuclear medicine specialist with 10 years of experience using a previously published protocol (21). MIM software (MIM Software Inc., Cleveland, OH, USA) was used to contour the nontumorous liver/liver parenchyma (referred to as "liver" in the remainder of this article) and the tumor margin on MR images (*Figure 2*). This was accomplished using a semi-automated method where manual contouring of the target lesion or liver lobe was performed on a single MR image of the PET/MR. Then, MIM software was able to automatically generate contours for the rest of the MR sequence. Manual adjustment was performed to fine-tune the contouring. MIM used rigid registration to align and fuse the attenuation-corrected PET images with contoured MR images. Voxel-based, volumetric dosimetry was automatically calculated using previously Food and Drug Administration (FDA)-approved and validated MIM SurePlan™ algorithm (22). The exact mathematical principles can be referenced from the recent MIM white paper (23). MR images were used for contouring because they offer better soft tissue resolution, superior demarcation of tumor margin, and superior demarcation of liver boundaries.

The contours were then transferred to the CT portion of the PET/CT to check for accuracy. If available, tumor contouring was also confirmed with intraprocedural cone beam CT by experienced interventional radiologists. If a discrepancy was suspected, the contours were fused with cone-beam CT images to further confirm the accuracy of contouring. MIM software fused the attenuation-corrected PET images with the contoured CT images, automatically obtaining voxel-based activities and volumes within the contoured margins.

Statistical analysis

Baseline variables such as demographics, patient body mass index, injected activity (GBq), and ROI volumes for liver and tumor were obtained. If multiple tumors were present, they were separated into multiple compartments and analyzed independently. Since the study was intended only for dosimetry method assessment, no additional patient demographic information was collected, including function status, disease burden, and liver function. Outcome variables included absorbed doses (Gy) for liver and tumor. Data were analyzed using SAS 9.4 (SAS Institute, Cary, NC, USA). Means and standard deviations (SDs) were determined for continuous variables, and percentages were determined for categorical variables. The Bland-Altman method was used to analyze the pattern of differences between dosimetry values obtained with the two modalities and to test the reproducibility of the methods. A generalized linear model was used to assess the effect of baseline variables on intermodality differences in adjusted absorbed doses, with generalized estimating equations used to account for multiple tumors in some patients. A P value <0.05 was considered statistically significant.

Results

The study population consisted of 12 men and 6 women; 2 of the women underwent 2 treatment sessions each. The

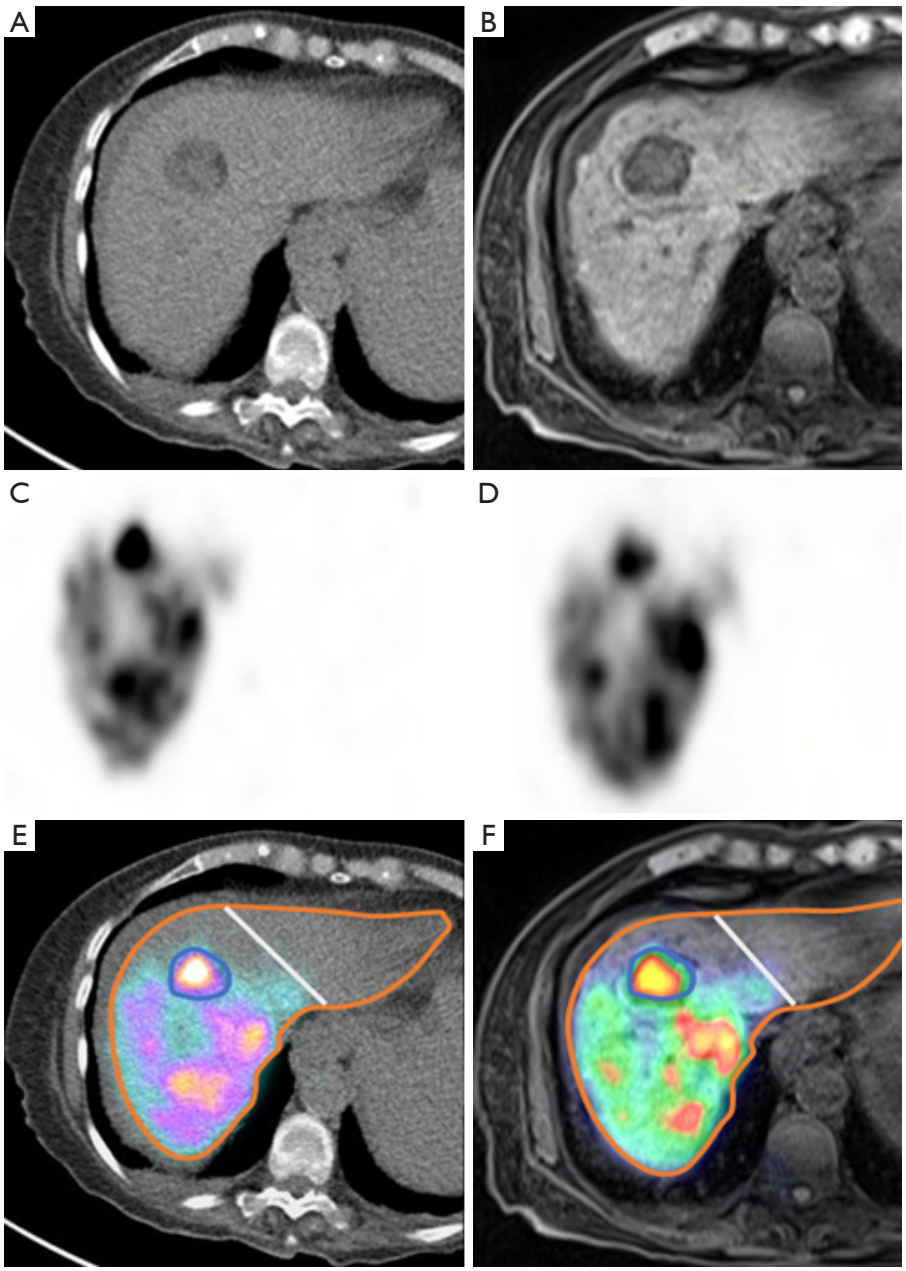

Figure 2 An example of treated tumor with radioembolization and subsequent PET/CT and PET/MR images. Noncontrast CT (A) and MR (B) images obtained after ^{90}Y radioembolization. Attenuation-corrected PET images derived from PET/CT (time-of-flight technique) (C) and derived from PET/MR (T1-weighted Dixon sequences leading to a 4-class segmentation model) (D). Fused PET/CT (E) and PET/MR (F) images with contours drawn around the liver (orange), tumor (blue), and lobe separation (white). PET, positron emission tomography; CT, computed tomography; MR, magnetic resonance.

mean age was 65 years (range, 48–84 years), and the mean baseline body mass index was 25.2±3.2 (range, 20.7–31.9). The injected activity ranged from 0.62 to 4.29 GBq. ROI volumes ranged from 3.5 to 798 mL for tumor (mean ± SD =142±197 mL) and from 512 to 2,536 mL for normal liver parenchyma (mean ± SD =1,156±494).

A total of 29 tumors were treated across the 20 treatment sessions. The prescribed radioembolic sphere injection

was planned to be lobar in 15 sessions, and radiation segmentectomy was pursued in 5 sessions. TheraSphere was used in 18 cases (90%), and SIR-Spheres were used in 2 cases (10%). Tumor types included 11 hepatocellular carcinomas (HCCs) (55%), 4 cholangiocarcinomas (20%), 2 melanoma metastases (10%), 2 neuroendocrine metastases (10%), and 1 colorectal cancer metastasis (5%). A representative case demonstrating the potential value of PET/MR to guide patient management is shown in *Figure 3*.

The liver-adjusted absorbed dose was 53.8±26.7 Gy for PET/CT and 50.7±25.4 Gy for PET/MR. The mean intermodality difference was –3.1 Gy [95% confidence interval (CI): –5.8 to –0.35 Gy; P=0.029], representing a –5.77% underestimation by PET/MR (*Figure 4A*). No significant correlation was found between the intermodality difference and liver parenchymal dose (r=–0.23; P=0.338, respectively). The percentage reproducibility coefficient was 26% (95% CI: 19.9% to 37.6%).

The tumor-adjusted absorbed dose was 259.7±179.7 Gy for PET/CT and 250.2±176.6 Gy for PET/MR. The mean intermodality difference was –9.6 Gy (95% CI: –18.8 to –0.34 Gy; P=0.042), representing a 3.65% underestimation by PET/MR (*Figure 4B*). There was no significant correlation between the tumor dose and intermodality difference (r=–0.13; P=0.502). The percentage reproducibility coefficient was 19.4% (95% CI: 15.4% to 26.1%). When comparing the coverage probability plot, 80% and 90% of tumor dose measurements fell within an intermodality difference of 11% and 18%, respectively (*Figure 5*).

The injected activity was significantly associated with intermodality dose differences (P<0.001). Body mass index and tumor volume were not significantly associated with intermodality dose differences (P=0.428 and 0.683, respectively). There was significant underestimation of tumor dose with PET/MR at both low (<1 GBq) and high (>3 GBq) injected activity levels (P<0.001) by –22.3 (SD =13.5) and –24.3 (SD =18.7) for nonlinear effect of injected activity, respectively) (*Figure 6*).

Discussion

To our knowledge, this is the first prospective study to assess PET/MR applicability and reproducibility for post-^{90}Y dosimetry. In this study, we compared post-^{90}Y radioembolization dosimetry between PET/MR and benchmark PET/CT and found PET/MR significantly underestimated tumor and liver absorbed doses, particularly at low and high injected activity levels.

Our findings were concordant with previous research. One previous study compared ^{18}F-fluorodeoxyglucose (^{18}F-FDG) PET/CT to PET/MR and found that the mean and maximum standardized uptake values were underestimated in the PET/MR group by approximately 10% (24). Another study demonstrated that PET/CT activity was 20% higher compared to PET/MR in patients undergoing ^{68}Ga-prostate-specific membrane antigen (PSMA) imaging (25). Similarly, a study including three different radiotracers (^{18}F-FDG, ^{18}F-ethylcholine, and ^{68}Ga-DOTATATE) revealed mean and maximum standardized uptake values that were 11% and 21% lower in the PET/MR group than in the PET/CT group (26). With regard to ^{90}Y dosimetry, a recent study demonstrated that PET/MR underestimated mean liver dose by approximately 10% in comparison to PET/CT (46.5±22.7 *vs.* 51.6±24.7 Gy, respectively, with a mean difference of 5.1±5.0 Gy). In this study, intermodality mean liver doses showed a difference of 18.5% or lower (27).

The underestimation of PET/MR activity level and absorbed dose can be attributed to differences in attenuation correction, ROI tracing, and possible uptake time bias. In our study, the ROI was the same for both PET/MR and PET/CT, which eliminated the effect of ROI tracing. Uptake time bias is commonly seen in radiotracers that undergo biodistribution, as longer scanning time allows for increased tracer accumulation within the target organ (28,29). Theoretically, ^{90}Y radioembolic microspheres do not undergo redistribution. Further, in our study, patients were randomized to undergo either PET/MR or PET/CT first, thus eliminating the effect of uptake time bias. Therefore, the intermodality differences are likely due to differences in attenuation correction, including effects from multichannel radiofrequency MR coils that are not included in the attenuation correction. In our study, the intermodality differences were lower than those seen in previous studies (3.6% and 5.8% versus approximately 10%). This is likely reflective of improvements in PET/MR attenuation correction techniques, as evidence has shown that better MR attenuation correction may lead to improvements in measured PET values (30,31). The PET/MR software (VE11) used in this study supports extended MR field-of-view imaging using the HUGE (B0 homogenization using gradient enhancement) sequence. This feature reduces the arm truncation artifact seen in standard Dixon images. The arm truncation artifact limits PET quantitative accuracy and introduces dosimetry errors. With a reduction in arm

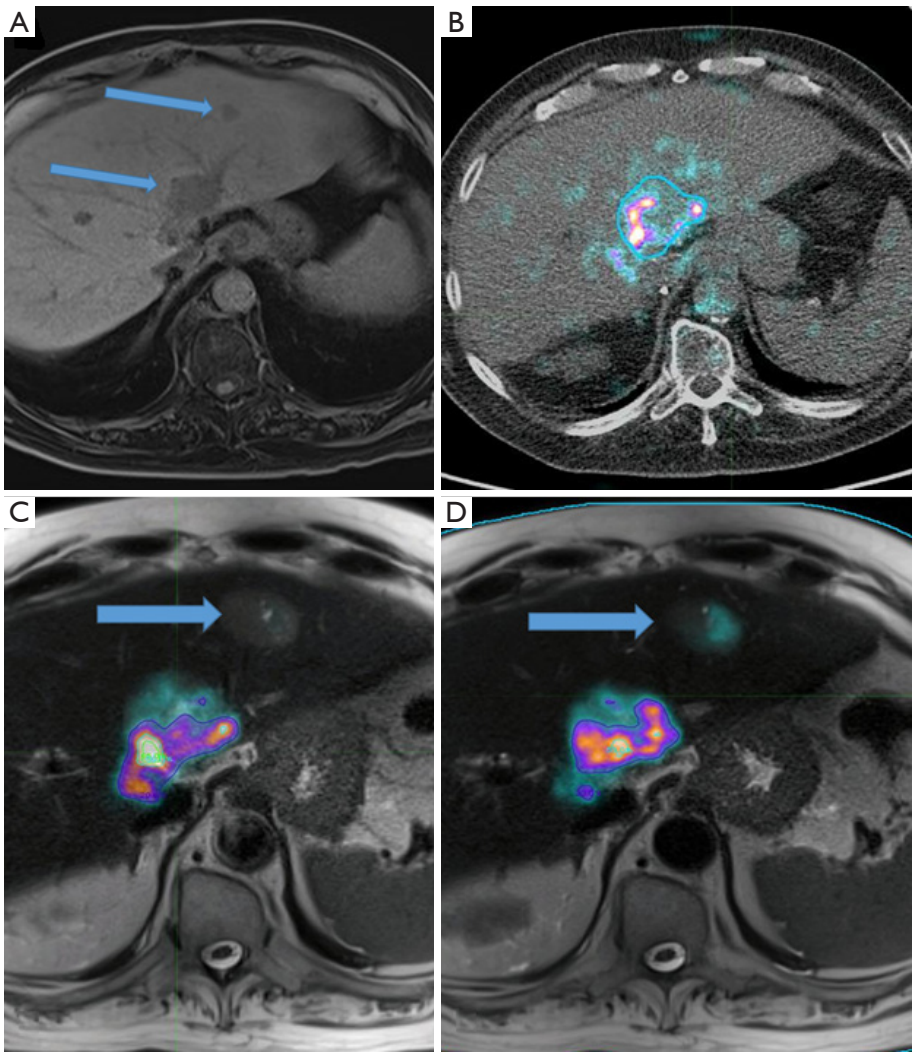

Figure 3 An example of treated tumor with radioembolization and subsequent PET/CT and PET/MR images. (A) Patient with prior partial right liver lobe resection who presented for ^{90}Y radioembolization of recurrent lesions in segments IVa and II (thin blue arrows). (B) Post-^{90}Y radioembolization PET/CT dosimetry suggested inadequate coverage of the segment IVa lesion and no coverage of the segment II lesion. Blue outline defined the boundary of the tumor. Based on these results, the decision was made to pursue a second ^{90}Y radioembolization treatment session. (C,D) Post-^{90}Y radioembolization PET/MR images obtained after the second treatment session clearly demonstrated an interval growth of the segment II lesion with suboptimal radiotracer coverage (thick blue arrows), as well as adequate treatment coverage of the segment IVa lesion based on the visual appearance and dosimetry calculations. As a result, the patient was referred for external beam radiation of the growing segment II lesion. There would have likely been a delay in treatment of this lesion had PET/MR not been performed. PET, positron emission tomography; CT, computed tomography; MR, magnetic resonance.

truncation artifact, the MR-based mu-map becomes more accurate, therefore improving PET/MR dosimetry.

In current clinical practice, ^{90}Y dosimetry is routinely performed prior to treatment, employing a variety of dosing models, including body surface area, Medical Internal Radiation Dosimetry, and the partition model. However, pretreatment dosimetry is inherently limited by several factors. Radioembolic microspheres are assumed to distribute uniformly within the treatment zone, an assumption that does not necessarily reflect clinical reality (32,33). Therefore, underdosing is common and may have resulted in underperformance of TARE in recent trials

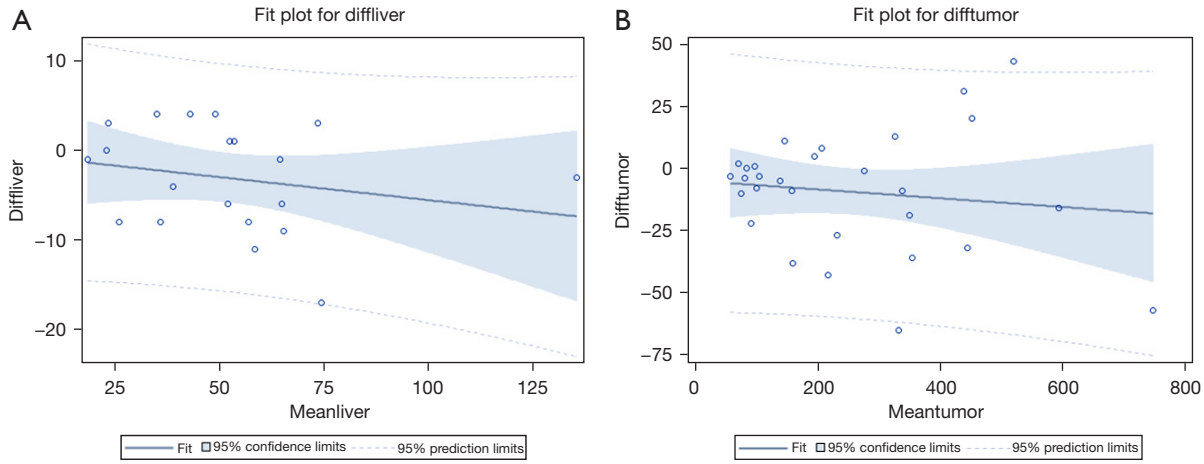

Figure 4 Various plots of intermodality differences at varying administered dose levels. (A) The diffliver was plotted against the meanliver. There was significant underestimation of liver dose with PET/MR but no significant trend between the underestimation and the magnitude of the liver dose (P=0.338). The mean underestimation was –3.1 (SD =5.9), with 95% CI of –5.8 to –0.35. (B) The difftumor was plotted against the meantumor. There was significant underestimation of tumor dose with PET/MR but no significant trend between the underestimation and the magnitude of the tumor dose (P=0.502). The mean underestimation was –9.4 (SD =24.1), with 95% CI of –18.8 to –0.34. PET, positron emission tomography; MR, magnetic resonance; SD, standard deviation; CI, confidence interval.

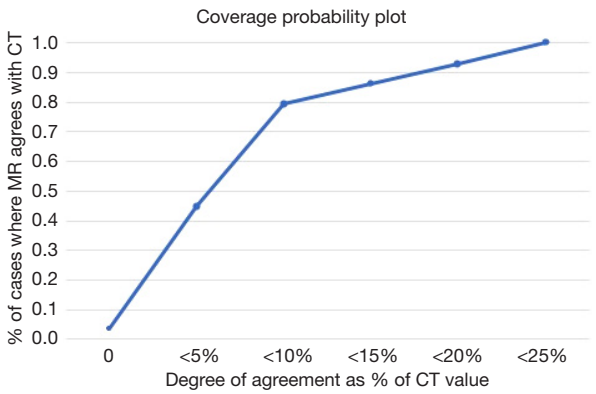

Figure 5 The degree of intermodality agreement was plotted against the degree of intermodality differences as a percentage of positron emission tomography/computed tomography value. At a difference of <18%, more than 90% intermodality agreement was achieved. MR, magnetic resonance; CT, computed tomography.

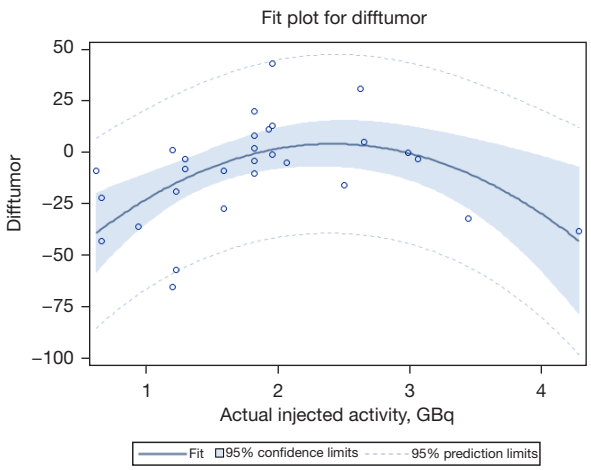

Figure 6 Intermodality differences in tumor dose measurements were plotted against the injected activity levels. There was significant underestimation of tumor dose with positron emission tomography/magnetic resonance at both low (<1 GBq) and high (>3 GBq) levels and little bias between 2 and 3 GBq (P<0.001 for nonlinear relationship), suggesting that the magnitude of underestimation depends on the injected activity level. difftumor, intermodality difference in tumor dose.

(34,35). More recently, a recent study has shown higher dosing threshold may be needed for optimal response (36), and personalized dosimetry has been shown to improve patient outcomes in comparison to standard dosing regimens, as shown in a prospective clinical trial (37).

In our study, post-treatment, voxel-based dosimetry could enable assessment of the actual dose distribution in an individual patient. However, it should be cautioned that these methods still remain imprecise, as the spatial

resolution of PET remains limited given the low positron count. In addition, hepatic dome lesion count measurement is inherently affected by patients' respiratory motion, which may require additional gating techniques (38). Previous studies demonstrated the value of post-treatment PET/CT dosimetry to predict threshold doses for liver toxicity (39), to assess for threshold doses for tumor response (40,41), and to reconstruct dose-volume histograms (42,43). In comparison to PET/CT, PET/MR is associated with decreased ionizing radiation exposure. Further, the superior soft tissue contrast resolution of MR imaging compared to CT allows for improved lesion detection. This allows not only for better assessment of desired target delivery, but also for identification of nontarget depositions, new or enlarging sites of hepatic malignant disease (as shown in *Figure 3*), and localization to portal vein thrombus that may not be apparent on unenhanced attenuation correction CT. The use of advanced noncontrast MR sequences such as diffusion-weighted imaging can also help assess therapy response from previous treatment or systemic therapy. Such information has implications for future treatment planning and is a potential benefit of PET/MR over PET/CT. This added value is the underlying rationale for further investigation of ways to optimize dosimetry calculations during PET-MR. However, there are also various challenges associated with PET/MR, including its limited access, its contraindication in patients with ferromagnetic implants or foreign bodies, its limited use in patients with claustrophobia, and its relatively longer acquisition times, as well as several technical challenges. In particular, MR-based attenuation correction algorithms are complex. Unlike PET/CT, in which attenuation correction is proportional to electron density, MR-based attenuation reflects the proton density and its relaxation time. MR-based attenuation correction is also affected by truncation artifacts/limited field of view, segmentation errors of bone and air, and MR artifacts secondary to implants and external devices/coils (44). A variety of techniques have been implemented to improve MR-based attenuation correction, including ultrashort echo time-based segmentation, inclusion of bone compartment, reduction of truncation artifact, and atlas-based methods (44). A previous feasibility study showed that PET/MR post-^{90}Y dosimetry enabled construction of dose-volume histograms as a predictor of treatment response (21). In a more recent study, investigators found that post-^{90}Y PET/MR dosimetry could be consistently obtained across multiple institutions on commercially available scanners if the tumor diameters were >22 mm, thus supporting the use of PET/MR as a method for obtaining accurate measurements across institutions (45).

This study had several limitations. PET/CT and PET/MR systems vary among vendors, so the findings from the current study may not apply to different PET/MR systems. For instance, our PET/MR scanner does not support PET TOF technique, which can enhance image quality. Additionally, the analysis included various hepatic malignant neoplasms, and prior research indicates that metastatic disease exhibits different radiosensitivities compared to primary HCC (46-48). Therefore, similar intermodality dose differences for primary HCC and other hepatic malignancies may have different effects on clinical outcomes, i.e., more radiosensitive tumors may be more prone to overdose or underdose in when using PET/MR-based dosimetry. Unfortunately, the sample size of this study was too small to permit separate intermodality difference analyses for various tumor types. Nevertheless, absorbed dose underestimation from post-treatment PET/MR dosimetry was lower when ^{90}Y injected activities were within 1 to 3 GBq. Although this study demonstrated that PET/MR significantly underestimated the absorbed dose in comparison to PET/CT, it remains unclear whether these differences are relevant with regard to patient care and outcomes.

Conclusions

The study found that PET/MR dosimetry significantly underestimated ^{90}Y absorbed dose compared to PET/CT for both the tumor and surrounding liver tissue. Intermodality differences were significant at both low (<1 GBq) and high (>3 GBq) injected activity levels. Post-treatment PET/MRI may be more suitable if injected activities fall outside these extremes. Further research is needed to externally validate these findings in both non-TOF and TOF-capable PET/MRI constructs and also to assess the impact our findings on patient care and outcomes.

Acknowledgments

We wish to thank Dr. David Faul from Siemens Medical Solutions, USA, for his valuable suggestions related to the prospective study design.

Funding: This study was investigator-initiated and was partially funded by a research grant from Cleveland Clinic Foundation Imaging Institute and by a research grant from Siemens Medical Solutions, USA.

Footnote

Reporting Checklist: The authors have completed the TREND reporting checklist. Available at https://jgo.amegroups.com/article/view/10.21037/jgo-23-890/rc

Data Sharing Statement: Available at https://jgo.amegroups.com/article/view/10.21037/jgo-23-890/dss

Peer Review File: Available at https://jgo.amegroups.com/article/view/10.21037/jgo-23-890/prf

Conflicts of Interest: All authors have completed the ICMJE uniform disclosure form (available at https://jgo.amegroups.com/article/view/10.21037/jgo-23-890/coif). All authors report that this study was partially funded by a research grant from Cleveland Clinic Foundation Imaging Institute and by a research grant from Siemens Medical Solutions, USA. The authors have no other conflicts of interest to declare.

Ethical Statement: The authors are accountable for all aspects of the work in ensuring that questions related to the accuracy or integrity of any part of the work are appropriately investigated and resolved. The study was conducted in accordance with the Declaration of Helsinki (as revised in 2013). The study was approved by the Institutional Review Board (IRB No. 20-232) and informed consent was obtained from all individual participants.

References

1. Rosenbaum CE, Verkooijen HM, Lam MG, et al. Radioembolization for treatment of salvage patients with colorectal cancer liver metastases: a systematic review. J Nucl Med 2013;54:1890-5.
2. Braat AJ, Smits ML, Braat MN, et al. ^{90}Y Hepatic Radioembolization: An Update on Current Practice and Recent Developments. J Nucl Med 2015;56:1079-87.
3. Flamen P, Vanderlinden B, Delatte P, et al. Multimodality imaging can predict the metabolic response of unresectable colorectal liver metastases to radioembolization therapy with Yttrium-90 labeled resin microspheres. Phys Med Biol 2008;53:6591-603.
4. Garin E, Rolland Y, Edeline J, et al. Personalized dosimetry with intensification using 90Y-loaded glass microsphere radioembolization induces prolonged overall survival in hepatocellular carcinoma patients with portal vein thrombosis. J Nucl Med 2015;56:339-46.
5. Riaz A, Lewandowski RJ, Kulik LM, et al. Complications following radioembolization with yttrium-90 microspheres: a comprehensive literature review. J Vasc Interv Radiol 2009;20:1121-30; quiz 1131.
6. Knesaurek K, Tuli A, Kim E, et al. Comparison of Y-90 dosimetry derived from post-therapy PET/CT and bremsstrahlung SPECT imaging. J Nucl Med 2016;57:1893.
7. Elschot M, Vermolen BJ, Lam MG, et al. Quantitative comparison of PET and Bremsstrahlung SPECT for imaging the in vivo yttrium-90 microsphere distribution after liver radioembolization. PLoS One 2013;8:e55742.
8. Strigari L, Sciuto R, Rea S, et al. Efficacy and toxicity related to treatment of hepatocellular carcinoma with 90Y-SIR spheres: radiobiologic considerations. J Nucl Med 2010;51:1377-85.
9. Rong X, Du Y, Ljungberg M, et al. Development and evaluation of an improved quantitative (90) Y bremsstrahlung SPECT method. Med Phys 2012;39:2346-58.
10. Kao YH, Steinberg JD, Tay YS, et al. Post-radioembolization yttrium-90 PET/CT - part 1: diagnostic reporting. EJNMMI Res 2013;3:56.
11. Selwyn RG, Nickles RJ, Thomadsen BR, et al. A new internal pair production branching ratio of 90Y: the development of a non-destructive assay for 90Y and 90Sr. Appl Radiat Isot 2007;65:318-27.
12. Lhommel R, van Elmbt L, Goffette P, et al. Feasibility of 90Y TOF PET-based dosimetry in liver metastasis therapy using SIR-Spheres. Eur J Nucl Med Mol Imaging 2010;37:1654-62.
13. Kao YH, Tan EH, Ng CE, et al. Yttrium-90 time-of-flight PET/CT is superior to Bremsstrahlung SPECT/CT for postradioembolization imaging of microsphere biodistribution. Clin Nucl Med 2011;36:e186-7.
14. Attarwala AA, Molina-Duran F, Büsing KA, et al. Quantitative and qualitative assessment of Yttrium-90

PET/CT imaging. PLoS One 2014;9:e110401.
15. Wright CL, Zhang J, Tweedle MF, et al. Theranostic Imaging of Yttrium-90. Biomed Res Int 2015;2015:481279.
16. Finnoff JT, Fowler SP, Lai JK, et al. Treatment of chronic tendinopathy with ultrasound-guided needle tenotomy and platelet-rich plasma injection. PM R 2011;3:900-11.
17. Partovi S, Kohan A, Rubbert C, et al. Clinical oncologic applications of PET/MRI: a new horizon. Am J Nucl Med Mol Imaging 2014;4:202-12.
18. Keereman V, Mollet P, Berker Y, et al. Challenges and current methods for attenuation correction in PET/MR. MAGMA 2013;26:81-98.
19. Kershah S, Partovi S, Traughber BJ, et al. Comparison of standardized uptake values in normal structures between PET/CT and PET/MRI in an oncology patient population. Mol Imaging Biol 2013;15:776-85.
20. Murthy R, Kamat P, Nuñez R, et al. Radioembolization of yttrium-90 microspheres for hepatic malignancy. Semin Intervent Radiol 2008;25:48-57.
21. Fowler KJ, Maughan NM, Laforest R, et al. PET/MRI of Hepatic 90Y Microsphere Deposition Determines Individual Tumor Response. Cardiovasc Intervent Radiol 2016;39:855-64.
22. Maughan NM, Garcia-Ramirez J, Arpidone M, et al. Validation of post-treatment PET-based dosimetry software for hepatic radioembolization of Yttrium-90 microspheres. Med Phys 2019;46:2394-402.
23. Piper J, Nelson A, Harper J. Deformable Image Registration in MIM Maestro Evaluation and Description. MIM Software. White Paper. Published March 2018.
24. Izquierdo-Garcia D, Sawiak SJ, Knesaurek K, et al. Comparison of MR-based attenuation correction and CT-based attenuation correction of whole-body PET/MR imaging. Eur J Nucl Med Mol Imaging 2014;41:1574-84.
25. Ringheim A, Campos Neto GC, Martins KM, et al. Reproducibility of standardized uptake values of same-day randomized (68)Ga-PSMA-11 PET/CT and PET/MR scans in recurrent prostate cancer patients. Ann Nucl Med 2018;32:523-31.
26. Wiesmüller M, Quick HH, Navalpakkam B, et al. Comparison of lesion detection and quantitation of tracer uptake between PET from a simultaneously acquiring whole-body PET/MR hybrid scanner and PET from PET/CT. Eur J Nucl Med Mol Imaging 2013;40:12-21.
27. Knešaurek K, Tuli A, Kim E, et al. Comparison of PET/CT and PET/MR imaging and dosimetry of yttrium-90 ((90)Y) in patients with unresectable hepatic tumors who have received intra-arterial radioembolization therapy with (90)Y microspheres. EJNMMI Phys 2018;5:23.
28. Matthiessen LW, Johannesen HH, Skougaard K, et al. Dual time point imaging fluorine-18 flourodeoxyglucose positron emission tomography for evaluation of large loco-regional recurrences of breast cancer treated with electrochemotherapy. Radiol Oncol 2013;47:358-65.
29. Matthies A, Hickeson M, Cuchiara A, et al. Dual time point 18F-FDG PET for the evaluation of pulmonary nodules. J Nucl Med 2002;43:871-5.
30. Oehmigen M, Lindemann ME, Gratz M, et al. Impact of improved attenuation correction featuring a bone atlas and truncation correction on PET quantification in whole-body PET/MR. Eur J Nucl Med Mol Imaging 2018;45:642-53.
31. Eldib M, Oesingmann N, Faul DD, et al. Optimization of yttrium-90 PET for simultaneous PET/MR imaging: A phantom study. Med Phys 2016;43:4768.
32. Högberg J, Rizell M, Hultborn R, et al. Increased absorbed liver dose in Selective Internal Radiation Therapy (SIRT) correlates with increased sphere-cluster frequency and absorbed dose inhomogeneity. EJNMMI Phys 2015;2:10.
33. Bourgeois AC, Chang TT, Bradley YC, et al. Intraprocedural yttrium-90 positron emission tomography/CT for treatment optimization of yttrium-90 radioembolization. J Vasc Interv Radiol 2014;25:271-5.
34. Tong AK, Kao YH, Too CW, et al. Yttrium-90 hepatic radioembolization: clinical review and current techniques in interventional radiology and personalized dosimetry. Br J Radiol 2016;89:20150943.
35. Wasan HS, Gibbs P, Sharma NK, et al. First-line selective internal radiotherapy plus chemotherapy versus chemotherapy alone in patients with liver metastases from colorectal cancer (FOXFIRE, SIRFLOX, and FOXFIRE-Global): a combined analysis of three multicentre, randomised, phase 3 trials. Lancet Oncol 2017;18:1159-71.
36. Palard X, Edeline J, Rolland Y, et al. Dosimetric parameters predicting contralateral liver hypertrophy after unilobar radioembolization of hepatocellular carcinoma. Eur J Nucl Med Mol Imaging 2018;45:392-401.
37. Garin E, Tselikas L, Guiu B, et al. Personalised versus standard dosimetry approach of selective internal radiation therapy in patients with locally advanced hepatocellular carcinoma (DOSISPHERE-01): a randomised, multicentre, open-label phase 2 trial. Lancet Gastroenterol Hepatol 2021;6:17-29.
38. Grimm R, Fürst S, Souvatzoglou M, et al. Self-gated MRI motion modeling for respiratory motion compensation in

integrated PET/MRI. Med Image Anal 2015;19:110-20.
39. Chan KT, Alessio AM, Johnson GE, et al. Hepatotoxic Dose Thresholds by Positron-Emission Tomography After Yttrium-90 Radioembolization of Liver Tumors: A Prospective Single-Arm Observational Study. Cardiovasc Intervent Radiol 2018;41:1363-72.
40. Song YS, Paeng JC, Kim HC, et al. PET/CT-Based Dosimetry in 90Y-Microsphere Selective Internal Radiation Therapy: Single Cohort Comparison With Pretreatment Planning on (99m)Tc-MAA Imaging and Correlation With Treatment Efficacy. Medicine (Baltimore) 2015;94:e945.
41. Chan KT, Alessio AM, Johnson GE, et al. Prospective Trial Using Internal Pair-Production Positron Emission Tomography to Establish the Yttrium-90 Radioembolization Dose Required for Response of Hepatocellular Carcinoma. Int J Radiat Oncol Biol Phys 2018;101:358-65.
42. Kao YH, Steinberg JD, Tay YS, et al. Post-radioembolization yttrium-90 PET/CT - part 2: dose-response and tumor predictive dosimetry for resin microspheres. EJNMMI Res 2013;3:57.
43. d'Abadie P, Walrand S, Hesse M, et al. Prediction of tumor response and patient outcome after radioembolization of hepatocellular carcinoma using 90Y-PET-computed tomography dosimetry. Nucl Med Commun 2021;42:747-54.
44. Izquierdo-Garcia D, Catana C. MR Imaging-Guided Attenuation Correction of PET Data in PET/MR Imaging. PET Clin 2016;11:129-49.
45. Maughan NM, Eldib M, Faul D, et al. Multi institutional quantitative phantom study of yttrium-90 PET in PET/MRI: the MR-QUEST study. EJNMMI Phys 2018;5:7.
46. van den Hoven AF, Rosenbaum CE, Elias SG, et al. Insights into the Dose-Response Relationship of Radioembolization with Resin 90Y-Microspheres: A Prospective Cohort Study in Patients with Colorectal Cancer Liver Metastases. J Nucl Med 2016;57:1014-9.
47. Eaton BR, Kim HS, Schreibmann E, et al. Quantitative dosimetry for yttrium-90 radionuclide therapy: tumor dose predicts fluorodeoxyglucose positron emission tomography response in hepatic metastatic melanoma. J Vasc Interv Radiol 2014;25:288-95.
48. Kao YH. Dose-response for yttrium-90 resin microsphere radioembolisation. Nucl Med Commun 2021;42:345-7.

Cite this article as: Gurajala R, Partovi S, DiFilippo FP, Li X, Coppa C, Shah SN, Karuppasamy K, Obuchowski N, Fayazzadeh E, McLennan G, Levitin A. Prospective comparison of positron emission tomography (PET)/magnetic resonance and PET/computed tomography dosimetry in hepatic malignant neoplastic disease after ^{90}Y radioembolization treatment. J Gastrointest Oncol 2024;15(1):356-367. doi: 10.21037/jgo-23-890

